High Efficiency Piezo-phototronic Solar Cells by Strain induced Polarization

Yaming Zhang[1], Jiaheng Nie[1], Baohua Teng[1*], Lijie Li [2, *] and Yan Zhang[1,3,4, *]

[1] School of Physics, University of Electronic Science and Technology of China, Chengdu 610054, China

[2] Multidisciplinary Nanotechnology Centre, College of Engineering, Swansea University, Swansea, SA1 8EN, UK

[3] Beijing Institute of Nanoenergy and Nanosystems, Chinese Academy of Sciences, Beijing 100083, China

[4] College of Nanoscience and Technology, University of Chinese Academy of Sciences, Beijing 100049, China

[*] To whom correspondence should be addressed, E-mail: phytbh@163.com, L.Li@swansea.ac.uk and zhangyan@uestc.edu.cn

Abstract

Toward theoretical power conversion efficiency (PCE) of two-dimensional (2D) material solar cell requires carrier and light management technologies. By strain-induced polarization of piezotronic and piezo-phototronic effect, under standard AM1.5G solar spectrum, the maximum theoretical power conversion efficiency of is 54.4% of SnS among the 2D piezoelectric semiconductors, such as SnS, MoS_2, GeS, WS_2, WSe_2, and $MoSe_2$. PCE of solar cell with 2D WS_2 and MoS_2 are boosted to 48.1% and 42.8%, respectively. Strain--induced polarization can not only increase built-in field, but also simplify bandgap gradients by inexpensive strain regulation. In this study, we propose the tandem and parallel piezo-phototronic solar cell (PSC) with single-type 2D piezoelectric semiconductor materials. This work provides a novel way to develop ultrahigh efficiency two-dimensional material solar cell.

Keywords: power conversion, strain-induced polarization, piezo-phototronic effect, piezo-phototronic solar cell

1. Introduction

Piezotronic and piezo-phototronic devices are novel properties of coupling of piezoelectricity, semiconductor, and photoexcitation [1-3]. Based on the third-generation semiconductors (such as CdS, ZnO, GaN, and monolayer chalcogenides) high performance piezotronic and piezo-phototronic devices are developed, such as nanogenerator[4-6], piezotronic strain sensor[7], piezotronic logic nanodevices[8], piezo-phototronic photodetectors[9], piezo-phototronic photocell[10], and LEDs[11]. Strain generated piezoelectric charges can adjust the process of carrier separation, transport and recombination [12]. Piezo-phototronic devices consisted of ZnO nanowires and single-layer MoS_2 can be used for highly sensitive force biological and medical imaging sensors [13-15]. Non-uniform strain can effectively enhance piezoelectric polarization to improve sensitivity of piezotronic devices[16]. The PCE of piezo-phototronic multijunction solar cell (PMJSC) theoretically has surpassed Shockley-Queisser (S-Q) limit [17].

The PCE limit of single-junction solar cell is calculated by detailed balance theory[18]. The photons energy absorbed by solar cell is above bandgap, while the carriers of energy equal to bandgap (E_g). The excess energy is thermalized. Various strategies are developed for increasing PCE, such as hot carrier collection[19], multiple exciton generation[20], and parallel (tandem) connection[21]. Tandem or parallel Multijunction solar cells (MJSC) consisting of different E_g junction can decrease the lattice thermalization losses[22]. MJSC has higher PCE than S-Q limit of single material, for example, PCE of tandem MJSC can exceed 47%[22-26]. However, MJSC face manufacturing and engineering complexity since different bandgap materials are mechanically stacked to build MJSC.

Strain can tune bandgap of semiconductor materials[27], and the stretching limit of monolayer 2D materials (including WS_2, MoS_2, GeS, WSe_2, etc) can reach 11% at in-plane strain[28]. Thus, 2D materials have a large enough E_g change by applying strain. Piezoelectric charges induced by strain can also control Schottky Barrier Height (SBH) to enhance or reduce PCE of PSC[29]. Previous work demonstrates the nonzero d_{33} in R-stacked transition metal dichalcogenides[30]. The PMJSC can be fabricated by vertically stacking. Thus, the single-type 2D materials for fabricating PMJSC of stacking different bandgap is holped to exceed S-Q limit and it possess valuably applications for utilizing simple engineering technology to design high performance solar cell.

In this study, the parallel and tandem PMJSC structures with single type 2D materials illustrated in figure 1 (a), (b). The different strain layer is as a single-junction cell. The stacked 2D materials absorbing a portion of photon energies in every junction. The spectral irradiance under AM1.5G solar spectrum is demonstrated in figure S1(a). The PCE of single-junction solar

cell changes with material E_g, the theoretical PCE limit is about 33%[31], shown in figure S1(b). The E_g of 2D materials is obviously modulated by strain; the 2D materials can have the wide range of bandgap for high PCE of solar spectrum. Two or three junction cells generally dominate the market because of less difficult of fabrication. Thus, the PMJSC also structures with three sub-cells and they severally adopt parallel and tandem architecture. Moreover, the different strain layer as sub-cells to realize bandgap reorganization. The piezo-charges can also optimize the thermalization loss owing to changing SBH. As a result, the PCE of parallel PMJSC based on WS_2 can arrive to 34%, and it slightly exceed the max S-Q limit. Significantly, the PCE of tandem PMJSC based on WS_2 can reach 48.1%, and it is theoretically break through designing ultrahigh efficiency solar cell. The PCE of parallel and tandem PMJSC with structures of single-type 2D materials (SnS, SnSe, GeS, GeSe, MoS_2, and so on) has been calculated. The PCE of PMJSC can generally exceed S-Q limit. Therefore, parallel and tandem PMJSC structure is both important developing directions to realize high efficiency solar cell.

2. Basic theory of two types of PMJSC

The PMJSC can enhance performance because of the piezoelectric potential and bandgap variety induced by strain. According to previous work, the ASTM has published standard AM1.5G spectrum for theoretical calculations.

In a parallel PMJSC, the structure and simplified equivalent circuit is similar to figure 1 (a). The total current density is equal to summation of current density of sub-cell. The $J-V$ characteristic of parallel PMJSC is[17]

$$\begin{cases} J(V)=\sum_{i=1}^{3}(J_0^i \exp(-\dfrac{qe_{11}s_{11}^i W_{piezo}}{2\varepsilon_s\varepsilon_0 kT_c})[\exp(\dfrac{qV}{kT_c})-1]-J_{sc}^i) \\ J_{sc}^p = J(V=0) \\ V_{oc}=V_{oc}^p+\dfrac{P_z W_{piezo}}{2\varepsilon_s\varepsilon_0} \end{cases} \quad (1)$$

where e_{11}, W_{piezo}, V, P_z, J_0^i, ε_s, ε_0, J_{sc}^i and J_{sc}^p is piezoelectric constant, piezoelectric charges distribution width, output voltage, piezoelectric polarization, reverse saturation current density of sub-cell, relative dielectric constant, vacuum dielectric constant, short circuit current density of sub-cell, the total short circuit current density, respectively. The V_{oc} and V_{oc}^p is open circuit voltage with and without piezo-charges.

For a tandem PMJSC, the structure and simplified equivalent circuit is shown in figure 1 (b). The total V_{oc} is equal to the summation of V_{oc} with sub-cell. The $J-V$ characteristic of tandem PMJSC is

$$\begin{cases} V(J) = \dfrac{kT_c}{q} \ln \prod_{i=1}^{3} \exp\left(\dfrac{q e_{11} s_{11}^i W_{piezo}}{2\varepsilon_s \varepsilon_0 kT_c}\right)\left(\dfrac{J_{sc}^i - J}{J_0^i} + 1\right) \\ V_{oc} = V_{oc}^T + \sum_{i=1}^{3} \dfrac{e_{11} s_{11}^i W_{piezo}}{2\varepsilon_s \varepsilon_0} \\ V(J = J_{sc}^T) = 0 \end{cases} \quad (2)$$

where V_{oc} and V_{oc}^T are open circuit voltage with or without piezo-charges. The detailed derivation is in supplementary.

From the equations of the model, the simulated device is a photodiode with metal-semiconductor contact. The mechanism that that drives the asymmetry mechanism for the preferential direction of the carriers is that a depletion region inside of photodiode owning high electric field, can separate photogenerated carriers[32, 33]. A PN junction with an internal electric field because of the depletion of carriers in some areas can be used for photodiode and solar cell. The asymmetry can be coming from different electrodes with contrasting work functions, this is the mechanism of metal-semiconductor contact. The model of current-voltage relationship can use a classical description of semiconductor drift-diffusion equations for the monolayer MoS_2 devices in experiments[34]. In this work, S-Q efficiency limit of the solar cell based on monolayer MoS_2 is descripted by semiconductor drift-diffusion equations[32, 33] . Lin, et, al show photovoltaic response of vdWs p–n diode by stacking few-layer p-WSe_2 and single-layer n-MoS_2, adopt classical semiconductor drift-diffusion equations to descript[35]. The photovoltaic response of 2D MoS_2 junction descripted by classical semiconductor drift-diffusion equations[36].The performance of 2D materials based solar cell is descripted by a combination of classical semiconductor drift-diffusion equations and DFT and the GW-Bethe Salpeter method for computing absorbance spectra with monolayers of graphene, WS_2, $MoSe_2$, and MoS_2[37]. The absorption spectra of MoS_2 is calculated by DFT[38]. The absorption spectra for monolayer MoS_2 is provided by HSE-G_0W_0-BSE ladder[39]. The parameters of materials can be calculated by DFT. The performance of the devices can simulate by classical semiconductor drift-diffusion.

Recently, the photovoltaic devices with n- and p-type vdW contacts present an V_{oc} of 0.6 V and PCE of 0.82%[40]. This work demonstrates Pd thin film on MoS_2 and Pt thin film on WSe_2 show work function 5.2 eV and 5.0 eV. The practical geometry of the cell: typical width and length of p-type few-layered WSe_2 vdW contact are W = 12 μm and L = 4 μm, respectively. The width and length of monolayer WSe_2 vdW contact is 4 μm and 1.5 μm. The parameters are used in our model. Our model mainly forces on detailed balance limit for PCE for most practical geometry of the cell. The model can be used for different electrodes, type of materials, and work function, which can be a comparative baseline without stress or strain[40]. The absorption

rate is probability of absorbing photons above bandgap E_g. The optical properties of mono- and few-layer two-dimensional materials can be characterized by three complementary spectroscopic techniques, including, photoluminescence (PL), optical absorption and photoconductivity. From absorption spectra, PL spectra, and photoconductivity spectra, absorption rate can be obtained for mono- and few-layer two-dimensional film. For simplicity, our model uses average absorption rate.

Wu et al. reported the first experiment of the piezoelectric output of two-dimensional MoS_2[41]. The odd number of layers MoS_2 flakes have piezoelectric output under stretching and releasing. For even number of layers MoS_2, no output is observed. The piezoelectric coefficients are measured by atomic force microscope (AFM) in a single layer of (MoS_2)[42]. The 3R-MoS_2 sheets display strong piezoelectric response, which is forbidden by the inversion symmetry owing to odd-even effect. These piezoelectric coefficients are not apparently dependent on the flake thickness[43-45]. The effective piezoelectric coefficient d_{33} of two-dimensional WS_2 was estimated by piezoelectric response force microscopy (PFM)[46-48]. The piezoelectric response of WS_2 nanosheets (~tens of nanometer) was measured by PFM[49, 50].

In the first experiment of the piezoelectric output of 2D MoS_2[41], while the substrate was bent, MoS_2 is applied strain with magnitude of uniaxial strain proportional to the inverse bending radius. The MoS_2 has piezoelectric output under strain along uniaxial direction. Above substrate bending method can easily operate the devices, and stress differently the different layers. The stress is applied by uniaxial direction for piezotronic and piezo-phototronic devices in the experiments[51-53]. Silicon based devices can generate strain gradient by AFM tip or tungsten probe to applied point force[54-56]. The MoS_2 junction is generated strain and strain gradient by AFM tip, the photovoltaic effect in the MoS_2 junctions is significantly enhanced[36].

Micromechanical exfoliation from bulk materials for atomically thin 2D TMDCs can used for fabricating the solar cell to avoid the screen of piezoelectric charges[57-60]. Flexible vdWs p–n diode is fabricated by stacking single-layer n-MoS_2 with few-layer p-WSe_2, which has obvious photovoltaic response[35]. Previous works[54-56] show the silicon-based devices is applied point force to generate strain gradient by using AFM tip or tungsten probe. The MoS_2 junction is induced strain by AFM tip, the photovoltaic effect in the MoS_2 junctions is significantly enhanced[36]. According to reference[61], periodic large strain gradients by selective hydrogen irradiation of bulk flakes. Thus, the flexible p–n diode is fabricated by stacking single-layer n-MoS_2 and few-layer p-WSe_2. The strain distribution can be controlled by utilizing AFM tip and tungsten probe.

Typical 2D material device structure is metal 2D material contact. For example, the MoS_2 metal contact shows perfect rectifying behavior, excellent photoresponsivity[34, 62]. The high optical quality monolayer WSe_2 p–n junctions were fabricated, generating bright

electroluminescence with smaller injection current of 1,000 times and 10 times smaller linewidth compared with MoS_2[63]. Pospischil et al. present a monolayer WS_2 p–n junction diode, as a photodiode and LED, photovoltaic cell, obtain electroluminescence efficiencies and light–power conversion of ~0.1% and ~0.5%[64], the scale is about 10 μm. Previous work[62] fabricated monolayer MoS_2 phototransistors with an order of 10 μm, demonstrate a maximum photoresponsivity of 880 AW^{-1} with 561 nm wavelength and a photoresponse in the range of 400–680 nm.

Figure 2 (a) shows the bandgap deformation potential (E_s) of different 2D materials. The bandgap deformation potential is the variety of bandgap by per 1% strain. The bandgap is nearly linear with strain for monolayer MoS_2, WS_2, GeSe, as shown in figure 2 (b). Other materials are shown in figure S2. Figure 2 (c) shows the PMJSC system, where increasing the strain could decrease the bandgap for the same 2D materials. Figure 2 (d) shows the ratio of e_{11} to ε_s , and E_g of different 2D piezoelectric materials and thin film piezoelectric semiconductor. The PCE of PMJSC is depend on material properties, the 2D materials of large e_{11}/ε_s can effectively tune SBH by strain. The PMJSC also need the large enough bandgap change of materials by strain. Thus, the PCE of PMJSC depend on the characteristics of 2D piezoelectric materials, such as piezoelectric constant, dielectric constant, bandgap, bandgap deformation potential. Therefore, Table 1 show the parameter of 2D piezoelectric semiconductor materials for calculating PCE of PMJSC.

3. Results and Discussion

The 2% strain for 2D materials layers (WS_2) is as top-cell, as shown in figure 3 (a). The E_g is approximately 1.42 eV. The V_{oc} , J_{sc} , and fill factor (FF) are important parameters for solar cells. For parallel PMJSC, J_{sc} , V_{oc} and FF can reach up 43.2 mA/cm^2, 0.90 V, and 87.3%, respectively. For tandem PMJSC, J_{sc} , V_{oc} and FF can reach up to 17.4 mA/cm^2, 3.05 V, and 90.5%, respectively. For parallel PMJSC, the J_{sc} is increased significantly, the V_{oc} and FF is decreased slightly as strain increases. For tandem PMJSC, the J_{sc} has optimum value particular strains due to the constraint of matching current. The V_{oc} is decreased, the FF is decreased slightly as strain increases. The V_{oc} , J_{sc} , and (FF) corresponding with figure 3-6 is shown in Figure S3-S8 (Supplementary Information), respectively. The PCE of parallel PMJSC depends on the strain change of 2D materials layers as middle and bottom cells. The highest PCE of parallel PMJSC could reach 34.0%, have surpassed the S-Q limit. Piezo-charges can tune SBH to reduce thermalization loss, a large enough bandgap change can make more photons is absorbed. There are bandgap reorganization and optimization of thermalization loss. The different fixed strain for 2D materials is as top-cell, as shown in figure 3 (b). The E_g is different

value, the change strain of 2D materials as middle and bottom cell. The PCE of parallel PMJSC can change, which depend on the strain change of top-cell and absorption rate. The 3% strain for 2D materials layers is as bottom-cell with the bandgap of 1.24eV, as depicted in figure 3 (c). The PCE of parallel PMJSC could change, depend on the strain change of 2D materials layers as top and middle cells. The max PCE of PMJSC can also reach 34.0%. The result is corresponded to figure 3 (a). They may have similar strain combination. As shown in figure 3 (d), the different fixed strain for 2D materials is as middle-cell, the E_g is different value, the change strain of 2D materials as top and middle cell, the PCE of parallel PMJSC can change, depend on the strain change of bottom-cell and absorption rate. The result is similar to figure 3 (b). The highest PCE will increase firstly and then decrease with strain layers of top/bottom sub-cell.

As shown in figure 4 (a), the 7% strain for 2D materials layers (WS_2) is as bottom-cell, the E_g is approximately 0.46 eV. the PCE of tandem PMJSC could change, depend on the strain change of 2D materials layers as top and middle cells. The max PCE of PMJSC can reach 46.6%. As shown in figure 4 (b), the different fixed strain for 2D materials is as bottom-cell, the E_g has different value, the change strain of 2D materials as top and middle cell, the PCE of tandem PMJSC can change, depend on the strain change of bottom-cell and absorption rate. The maximum PCE of tandem PMJSC will appear at the strain of bottom-cell from 5% to 7%. While the strain of bottom cell is lower than 3%, the low absorption rate of every junction can have high PCE, and this is because of current matched. The maximum PCE of tandem PMJSC will first enhance with increasing the strain at bottom cell from 0 to 5% and then have a slight decline at increasing strain of bottom cell from 5% to 7%. The maximum PCE may also appear close to 0 at some strain combination owing to current matched of every junction. Thus, this result is because of piezo-phototronic effect, deformation potential and current matched.

Figure 5 demonstrates the photons absorption rate can also affect the PCE of PMJSC. As shown in Figure 5 (a), the maximum PCE of parrel PMJSC will increase with enhancing absorption rate. Figure 5 (b) show the maximum PCE of the parallel PMJSC change with photons absorption rate of every junction. and the maximum PCE will appear at bottom cell of 1% to 3% strain. This is owing to strain reorganization and optimization of thermalization loss by strain. As shown in figure 5 (c), the strain of 2D materials layer is lower than 2% as top-cell, the maximum PCE of tandem PMJSC increase with increasing photons absorption rate, and the PCE can achieve 48.1%. While the strain of top-cell layer is higher than 2%, the PCE will have extreme value at absorption rate about 0.5. Figure 5 (d) show the maximum PCE of tandem PMJSC can change with photons absorption rate of every junction, the maximum PCE (over 46.6%) will appear while strain of bottom cell layer from 5% to 7%. While the strain of bottom-cell layer is higher than 3%, the maximum PCE will increase with enhancing absorption rate,

and it surpasses the S-Q limit. While the strain of top cell layer is lower than 3%, the PCE will have extreme value at absorption rate about 0.5. This is caused by piezo-phototronic effect, deformation potential and current matching. Thus, the PCE is affected since the strain of sub-cell layer and absorption rate both affect current matching of PMJSC.

Figure 6 (a) and (b) demonstrate the maximum PCE of parallel and tandem PMJSC for different 2D materials. The maximum PCE of parallel PMJSC is steadily comparing with the tandem PMJSC. However, the tandem PMJSC has higher PCE. Some 2D materials (such as WSe_2, GeS, SnS, WS_2, and MoS_2) all have ultrahigh PCE for both parallel and tandem PMJSC. Some 2D materials (such as $MoSe_2$) only have high PCE for parallel PMJSC. The highest PCE of tandem and parallel PMJSC for other two-dimensional materials (sach as SnSe and GeSe) is inferior comparing with the above materials. Figure 6 (c) show the maximum PCE of parallel PMJSC change with bandgap, deformation potential and piezoelectric performance, respectively. The highest PCE is generally large while the initial bandgap is large and the deformation is smaller. The abnormal case is because of weaker piezoelectric performance (such as WSe_2 comparing with GeSe). Figure 6 (d) show the maximum PCE of tandem PMJSC change with bandgap, deformation potential and piezoelectric performance. The maximum PCE is high while the bandgap and the deformation is both large. the abnormal case is because of stronger piezoelectric performance (such as SnS and GeS).

Previous experiments measured the performance of stiffness and breaking strength with single-layer MoS_2. The average breaking strength of single-layer MoS_2 is 15±3 Nm^{-1} (23 GPa). With effective strain of 6 and 11%, breaking occurs [28]. Because the theoretical PCE of solar cell is around 1.2 eV[18]. In our model, the band gap changes with the strain from previous experimental and theoretical data. The high efficiency is 1.12 eV from experiments[65]. The strain of 2% is to be as close as possible to an optimum bandgap.

The PCE of PSC is increased by the strain generated piezo-potential[29]. The thin film piezoelectric semiconductor is used for fabricating PSC cell and PMJSC[66-68]. The performance of piezo-phototronic thin film solar cell have been studied. The PCE is enhance by 17.1% at 0.32% tensile strain. Piezo-phototronic effect can improve the PCE of 2D materials. The principle can be easily fabricated in GaN or ZnO thin film devices. Performance of ZnO/perovskite solar cells is obviously enhanced by piezo-phototronic effect, with the V_{oc} improved by 25.42%, the I_{sc} improved by 629.47%, and PCE improved by 1280% (from 0.0216% to 0.298%) [69]. Under vertical pressure, the piezo-phototronic effect can promote PCE of n-ZnO/p-SnS core–shell nanowire array solar cell for 37.3%.[70]. The J_{sc} and the PCE of solar cells with InGaN/GaN multiple quantum well increased by stress[71, 72].

For ideal PMJSC, the efficiency of S-Q limit is changed with bandgap[18]. In our theoretical model for WS_2, the PCE, J_{sc} ,V_{oc} and FF without mechanical stress are 26.6%, 19.4 mA/cm^2, 1.50 V, and 91.4%, respectively. In the experiments, without mechanical stress, the PCE of solar cell of SnS, SnSe, GeS, GeSe, WS_2, WSe_2, MoS_2, $MoSe_2$ are 4.8%[73], 6.34%[74], 1.36%[75], 5.2%[76], 3.3%[77], 5.1%[78], 2.8%[79], 0.5%[80], respectively. Thus, this can also highlight improvements of cells that do not overcome the S-Q limit, but overperform significantly the cells that do not have any mechanical stress. For perovskite structure, perovskite solar cells without mechanical stress achieved PCE of 25% under simulated AM1.5 illumination[81]. The certified PCE has been reported to 29.5%, with perovskite/Si tandem cell[31].

The new structure of tandem PMJSC has been designed, and two-dimensional SnS, SnSe, GeS, GeSe, WS_2, WSe_2, $MoSe_2$ have been calculated in this work, compared to MoS_2 in reference [5] in the SI. We explain this carefully in the Introduction. According to previous theories and experiments[82, 83], the tandem PMJSC demands current-matching, the parallel PMJSC demands voltage-matching. The optimum PCE of parallel and tandem PMJSC depend on bandgap, piezoelectric constant, dielectric constant, and bandgap deformation potential. This work provides a new method for designing high PCE PMJSC.

4. Conclusion

We present the theoretical model of tandem and parallel PMJSC structures with single-type 2D piezoelectric materials, the different strain layer is as every single junction. The work mechanism of two type of PMJSC is investigated. The piezoelectric charges and deformation potential jointly modulate J_{sc} and V_{oc} to tune PCE of PMJSC. The PCE of parallel and tandem PMJSC is calculated based on detail balance limit. Under standard AM1.5G solar spectrum, the PCE of parallel PMJSC based on MoS_2 can reach 42.8%, it has exceeded the S-Q limit. The PCE of tandem PMJSC based on WS_2 can theoretically reach to 48.1%, and the PCE vastly surpass the S-Q limit. We also simulate the PCE of parallel and tandem PMJSC for different single-type 2D materials (SnS, SnSe, GeS, GeSe, MoS_2, and so on). The PCE of PMJSC can generally surpass S-Q limit. We also analysis factor of affecting the PCE of parallel and tandem PMJSC (such as, initial bandgap, deformation potential, and piezoelectric performance). This work provides a method to realize high efficiency solar cells because of bandgap reorganization and optimization by strain, and helps research screen 2D piezoelectric semiconductor to fabricate the ultrahigh efficiency PMJSC.

On behalf of all authors, the corresponding author states that there is no conflict of interest.

Acknowledgments

The authors are thankful for the support from Major Project of National Natural Science Foundation of China (Grant No. 52192612, 52192610). The authors are thankful for the support from University of Electronic Science and Technology of China (grant no. ZYGX2021YGCX001).

Figure caption

Figure 1 Schematic of PMJSC based on 2D piezoelectric semiconductor materials. (a) Parallel; (b) Tandem. The inserts show schematic presentation of all the layers consisting PMJSC and equivalent circuit of PMJSC.

Figure 2 (a) bandgap deformation potential (E_s) of different 2D materials. (b) Bandgap as a function of strain for monolayer MoS_2, WS_2, GeSe. (c) Piezo-charges as a relation of strain; (d) Ratio of piezoelectric constant to dielectric constant, bandgap for different 2D piezoelectric materials and thin film piezoelectric semiconductor.

Figure 3 (a) the strain of top cell layer is 2%, PCE of parallel PMJSC change with strain of middle and bottom cell; (b) the strain of middle and bottom cell layer is changed, the max PCE as function with strain of top cell layer and absorption rate. (c) the strain of bottom cell layer is 3%, PCE of parallel PMJSC vary with strain of top and middle cell; (d) the strain of top and middle cell layer is changed, the highest PCE as function with the strain of top cell and absorption rate.

Figure 4 (a) The fixed strain of bottom cell is 7%, PCE of tandem PMJSC cell change with strain of top and middle cell. (b) The optimum PCE point at different strain of bottom-cell.

Figure 5. The optimum PCE point of parallel PMJSC at different absorption rate: (a) The different strain of top cell; (b) The different strain of bottom cell. The optimum PCE point of tandem PMJSC at different absorption rate: (c) The different strain of top cell; (d) The different strain of bottom cell.

Figure 6 (a) the optimum PCE of parallel PMJSC for different 2D materials. (b) the optimum PCE of tandem PMJSC for different 2D materials. the optimum PCE of (c) parallel and (d) tandem PMJSC change with bandgap and bandgap deformation potential. The sentence “ $\mathbf{S}_{11}^{m}$ is the maximum value of the optimum set of strain.

Table

Table 1. Bandgap, dielectric constant, deformation potential, and piezoelectric constant of some 2D piezoelectric semiconductor materials

Materials	E_g**(eV)**	ε_s	E_s**(meV)**	e_{11}**(C/m^2)**
SnS	1.63[84]	15.78[85]	116.00[84]	4.11[86, 87]
SnSe	1.05[88]	17.95[85]	87.5.00[88]	4.26[86, 87]
GeS	1.60[89]	11.75[90]	160.00[89]	1.36[86, 87]
GeSe	1.16[91]	10.10[90]	145.00[91]	2.37[86, 87]
WS_2	1.81[92]	5.80[93]	193.75[92]	0.40[94, 95]
WSe_2	1.49[92]	4.63[39]	140.00[92]	0.42[14, 94]
MoS_2	1.82[96]	3.30[97]	59.00[96]	0.56[95]
$MoSe_2$	1.58[98]	4.74[39]	27.00[98]	0.61[92, 94]

Table 2 PCE of parallel and tandem PMJSC for 2D piezoelectric semiconductor materials

Materials	**PMJSC (parallel)**				**PMJSC (tandem)**				e_{11}/ε	**Range of E_g tuned by strain**
	PCE (%)	J_{sc} (mA/cm^2)	V_{oc} (V)	FF (%)	PCE (%)	J_{sc} (mA/cm^2)	V_{oc} (V)	FF (%)		
SnS	40.8	51.6	0.91	87.3	54.4	21.0	2.91	89.0	0.26	0.35-1.63
SnSe	32.1	51.5	0.73	85.4	24.2	14.0	1.96	88.2	0.24	0.09-1.05
GeS	34.6	43.6	0.91	87.3	45.4	20.6	2.50	88.3	0.16	0.16-1.60
GeSe	32.6	43.7	0.82	90.8	27.1	15.2	2.03	87.8	0.23	0.15-1.16
WS_2	34.0	43.2	0.90	87.3	48.1	17.4	3.05	90.5	0.07	0.07-1.81
WSe_2	33.9	43.4	0.86	90.6	39.1	18.9	2.34	88.4	0.09	0.09-1.49
MoS_2	42.8	41.0	1.16	89.6	41.9	11.4	3.97	92.4	0.17	1.17-1.82
$MoSe_2$	38.9	35.6	1.22	89.9	26.3	7.62	3.73	92.8	0.13	1.28-1.58

Table 3 PCE of PMJSC and solar cell with no mechanical stress for 2D piezoelectric semiconductor materials

Materials	PMJSC (parallel)				PMJSC (tandem)				Single Gap (PCE)	
	PCE (%)	J_{sc} (mA/cm^2)	V_{oc} (V)	FF (%)	PCE (%)	J_{sc} (mA/cm^2)	V_{oc} (V)	FF (%)	Theory (%)	Expt. (%)
SnS	40.8	51.6	0.91	87.3	54.4	21.0	2.91	89.0	29.8	4.80[73]
SnSe	32.1	51.5	0.73	85.4	24.2	14.0	1.96	88.2	31.1	6.34[74]
GeS	34.6	43.6	0.91	87.3	45.4	20.6	2.50	88.3	30.0	1.36[75]
GeSe	32.6	43.7	0.82	90.8	27.1	15.2	2.03	87.8	32.8	5.20[76]
WS_2	34.0	43.2	0.90	87.3	48.1	17.4	3.05	90.5	26.6	3.30[77]
WSe_2	33.9	43.4	0.86	90.6	39.1	18.9	2.34	88.4	31.7	5.10[78]
MoS_2	42.8	41.0	1.16	89.6	41.9	11.4	3.97	92.4	26.5	2.80[79]
$MoSe_2$	38.9	35.6	1.22	89.9	26.3	7.62	3.73	92.8	30.4	0.50[80]

Reference

[1] W. Wu and Z.L. Wang, Nature Reviews Materials. 1, (2016). http://doi.org/10.1038/natrevmats.2016.31

[2] Z.L. Wang, W. Wu and C. Falconi, MRS Bulletin. 43, 922 (2018). http://doi.org/10.1557/mrs.2018.263

[3] C. Pan, J. Zhai and Z.L. Wang, Chem Rev. 119, 9303 (2019). http://doi.org/10.1021/acs.chemrev.8b00599

[4] Z.L. Wang and J. Song, Science. 312, 242 (2006). http://doi.org/10.1126/science.1124005

[5] X. Wang, J. Song, J. Liu, and Z.L. Wang, Science. 316, 102 (2007). http://doi.org/10.1126/science.1139366

[6] Y. Qin, X. Wang and Z.L. Wang Nature. 451, 809 (2008). http://doi.org/10.1038/nature06601

[7] J. Zhou., Y. Gu., P. Fei., W. Mai., Y. Gao., R. Yang., G. Bao., and Z.L. Wang., Nano letters. 8, 3035 (2008).

[8] W. Wu, Y. Wei and Z.L. Wang, Adv Mater. 22, 4711 (2010). http://doi.org/10.1002/adma.201001925

[9] Q. Yang, X. Guo, W. Wang, Z. Yan, X. Sheng, L. Der Hsien, and W. Zhong Lin, Acs Nano. 4, 6285 (2010).

[10] Y. Hu, Y. Zhang, Y. Chang, Robert L. Snyder, and W. Zhong Lin, ACS Nano. 4220 (2010).

[11] Q. Yang, W. Wang, S. Xu, and Z.L. Wang, Nano Lett. 11, 4012 (2011). http://doi.org/10.1021/nl202619d

[12] Y. Zhang, Y. Leng, M. Willatzen, and B. Huang, MRS Bulletin. 43, 928 (2018). http://doi.org/10.1557/mrs.2018.297

[13] Y. Zhang and L. Li, Nano Energy. 22, 533 (2016). http://doi.org/10.1016/j.nanoen.2016.02.039

[14] L. Li and Y. Zhang, Nano Research. 10, 2527 (2017). http://doi.org/10.1007/s12274-017-1457-y

[15] Y. Zhang, J. Nie and L. Li, Nano Research. 11, 1977 (2018). http://doi.org/10.1007/s12274-017-1814-x

[16] Y. Zhang, G. Hu, Y. Zhang, L. Li, M. Willatzen, and Z.L. Wang, Nano Energy. 60, 649 (2019). http://doi.org/10.1016/j.nanoen.2019.04.011

[17] G. Michael, Y. Zhang, J. Nie, D. Zheng, G. Hu, R. Liu, M. Dan, L. Li, and Y. Zhang, Nano Energy. 76, (2020). http://doi.org/10.1016/j.nanoen.2020.105091

[18] W. Shockley and H.J. Queisser, Journal of Applied Physics. 32, 510 (1961). http://doi.org/10.1063/1.1736034

[19] D. König, K. Casalenuovo, Y. Takeda, G. Conibeer, J.F. Guillemoles, R. Patterson, L.M. Huang, and M.A. Green, Physica E: Low-dimensional Systems and Nanostructures. 42, 2862 (2010). http://doi.org/10.1016/j.physe.2009.12.032

[20] M.C. Beard, J Phys Chem Lett. 2, 1282 (2011). http://doi.org/10.1021/jz200166y

[21] A.D. Vos, J. Phys. D: Appl. Phys. 13, 83946 (1980).

[22] C.H. Henry, Journal of applied physics. 51, 4494 (1980).

[23] A.S. Brown and M.A. Green, Physica E: Low-dimensional Systems and Nanostructures. 14, 96 (2002).

[24] J.P. Connolly, D. Mencaraglia, C. Renard, and D. Bouchier, Progress in Photovoltaics: Research and Applications. 22, 810 (2014).

[25] S. Abdul Hadi, E.A. Fitzgerald and A. Nayfeh, Journal of Applied Physics. 119, 073104 (2016).

[26] J.F. Geisz, R.M. France, K.L. Schulte, M.A. Steiner, A.G. Norman, H.L. Guthrey, M.R. Young, T. Song, and T. Moriarty, Nature Energy. 5, 326 (2020). http://doi.org/10.1038/s41560-020-0598-5

[27] J. Feng, X. Qian, C.-W. Huang, and J. Li, Nature Photonics. 6, 866 (2012).

[28] S. Bertolazzi, J. Brivio and A. Kis, ACS Nano. 5, 9703 (2011). http://doi.org/10.1021/nn203879f

[29] Y. Zhang, Y. Yang and Z.L. Wang, Energy & Environmental Science. 5, 6850 (2012). http://doi.org/10.1039/c2ee00057a

[30] L. Rogée, L. Wang, Y. Zhang, S. Cai, P. Wang, M. Chhowalla, W. Ji, and S.P. Lau, Science. 376, 973 (2022).

[31] R. Wang, T. Huang, J. Xue, J. Tong, K. Zhu, and Y. Yang, Nature Photonics. 15, 411 (2021). http://doi.org/10.1038/s41566-021-00809-8

[32] S.M. Sze, Y. Li and K.K. Ng, Physics of semiconductor devices. (John wiley & sons.2021)

[33] J.A. Nelson, The physics of solar cells. (World Scientific Publishing Company.2003)

[34] X. Zhang, Q. Liao, S. Liu, Z. Kang, Z. Zhang, J. Du, F. Li, S. Zhang, J. Xiao, B. Liu, Y. Ou, X. Liu, L. Gu, and Y. Zhang, Nat Commun. 8, 15881 (2017). http://doi.org/10.1038/ncomms15881

[35] P. Lin, L. Zhu, D. Li, L. Xu, C. Pan, and Z. Wang, Advanced Functional Materials. 28, (2018). http://doi.org/10.1002/adfm.201802849

[36] P. Chaudhary, H. Lu, M. Loes, A. Lipatov, A. Sinitskii, and A. Gruverman, Nano Lett. 22, 1047 (2022). http://doi.org/10.1021/acs.nanolett.1c04019

[37] M. Bernardi, M. Palummo and J.C. Grossman, Nano Lett. 13, 3664 (2013). http://doi.org/10.1021/nl401544y

[38] D.Y. Qiu, F.H. da Jornada and S.G. Louie, Phys Rev Lett. 111, 216805 (2013). http://doi.org/10.1103/PhysRevLett.111.216805

[39] A. Ramasubramaniam, Physical Review B. 86, 115409 (2012).

[40] Y. Wang, J.C. Kim, Y. Li, K.Y. Ma, S. Hong, M. Kim, H.S. Shin, H.Y. Jeong, and M. Chhowalla, Nature. 610, 61 (2022). http://doi.org/10.1038/s41586-022-05134-w

[41] W. Wu, L. Wang, Y. Li, F. Zhang, L. Lin, S. Niu, D. Chenet, X. Zhang, Y. Hao, T.F. Heinz, J. Hone, and Z.L. Wang, Nature. 514, 470 (2014). http://doi.org/10.1038/nature13792

[42] H. Zhu, Y. Wang, J. Xiao, M. Liu, S. Xiong, Z.J. Wong, Z. Ye, Y. Ye, X. Yin, and X. Zhang, Nat Nanotechnol. 10, 151 (2015). http://doi.org/10.1038/nnano.2014.309

[43] T. Dan, M. Willatzen and Z.L. Wang, Nano Energy. 56, 512 (2019). http://doi.org/10.1016/j.nanoen.2018.11.073

[44] H. Hallil, W. Cai, K. Zhang, P. Yu, S. Liu, R. Xu, C. Zhu, Q. Xiong, Z. Liu, and Q. Zhang, Advanced Electronic Materials. 2101131 (2022).

[45] W. Cai, J. Wang, Y. He, S. Liu, Q. Xiong, Z. Liu, and Q. Zhang, Nanomicro Lett. 13, 74 (2021). http://doi.org/10.1007/s40820-020-00584-1

[46] Y.-X. Zhou, Y.-T. Lin, S.-M. Huang, G.-T. Chen, S.-W. Chen, H.-S. Wu, I.C. Ni, W.-P. Pan, M.-L. Tsai, C.-I. Wu, and P.-K. Yang, Nano Energy. 97, (2022). http://doi.org/10.1016/j.nanoen.2022.107172

[47] L. Li, P. Wen, Y. Yang, N. Huo, and J. Li, Journal of Materials Chemistry C. 9, 1396 (2021). http://doi.org/10.1039/d0tc05001f

[48] C.J. Brennan, R. Ghosh, K. Koul, S.K. Banerjee, N. Lu, and E.T. Yu, Nano Lett. 17, 5464 (2017). http://doi.org/10.1021/acs.nanolett.7b02123

[49] R. Cao, R. Wu, D. Zhang, and S. Xu, Applied Surface Science. 553, (2021). http://doi.org/10.1016/j.apsusc.2021.149557

[50] Q. Truong Hoang, K.A. Huynh, T.G. Nguyen Cao, J.H. Kang, X.N. Dang, V. Ravichandran, H.C. Kang, M. Lee, J.E. Kim, Y.T. Ko, T.I. Lee, and M.S. Shim, Adv Mater. e2300437 (2023). http://doi.org/10.1002/adma.202300437

[51] W. Wu, X. Wen and Z.L. Wang, Science. 340, 952 (2013).

[52] C. Pan, L. Dong, G. Zhu, S. Niu, R. Yu, Q. Yang, Y. Liu, and Z.L. Wang, Nature Photonics. 7, 752 (2013). http://doi.org/10.1038/nphoton.2013.191

[53] L. Wang, S. Liu, X. Feng, Q. Xu, S. Bai, L. Zhu, L. Chen, Y. Qin, and Z.L. Wang, ACS Nano. 11, 4859 (2017). http://doi.org/10.1021/acsnano.7b01374

[54] S.M. Park, B. Wang, T. Paudel, S.Y. Park, S. Das, J.R. Kim, E.K. Ko, H.G. Lee, N. Park, L. Tao, D. Suh, E.Y. Tsymbal, L.Q. Chen, T.W. Noh, and D. Lee, Nat Commun. 11, 2586 (2020). http://doi.org/10.1038/s41467-020-16207-7

[55] L. Wang, S. Liu, X. Feng, C. Zhang, L. Zhu, J. Zhai, Y. Qin, and Z.L. Wang, Nat Nanotechnol. 15, 661 (2020). http://doi.org/10.1038/s41565-020-0700-y

[56] D. Guo, P. Guo, L. Ren, Y. Yao, W. Wang, M. Jia, Y. Wang, L. Wang, Z.L. Wang, and J. Zhai, Science Advances. 9, eadd3310 (2023).

[57] K.S. Novoselov, D. Jiang, F. Schedin, T. Booth, V. Khotkevich, S. Morozov, and A.K. Geim, Proceedings of the National Academy of Sciences. 102, 10451 (2005).

[58] K.F. Mak, C. Lee, J. Hone, J. Shan, and T.F. Heinz, Phys Rev Lett. 105, 136805 (2010). http://doi.org/10.1103/PhysRevLett.105.136805

[59] B. Radisavljevic, A. Radenovic, J. Brivio, V. Giacometti, and A. Kis, Nat Nanotechnol. 6, 147 (2011). http://doi.org/10.1038/nnano.2010.279

[60] Q.H. Wang, K. Kalantar-Zadeh, A. Kis, J.N. Coleman, and M.S. Strano, Nat Nanotechnol. 7, 699 (2012). http://doi.org/10.1038/nnano.2012.193

[61] E. Blundo, C. Di Giorgio, G. Pettinari, T. Yildirim, M. Felici, Y. Lu, F. Bobba, and A. Polimeni, Advanced Materials Interfaces. 7, (2020). http://doi.org/10.1002/admi.202000621

[62] O. Lopez-Sanchez, D. Lembke, M. Kayci, A. Radenovic, and A. Kis, Nat Nanotechnol. 8, 497 (2013). http://doi.org/10.1038/nnano.2013.100

[63] J.S. Ross, P. Klement, A.M. Jones, N.J. Ghimire, J. Yan, D.G. Mandrus, T. Taniguchi, K. Watanabe, K. Kitamura, W. Yao, D.H. Cobden, and X. Xu, Nat Nanotechnol. 9, 268 (2014). http://doi.org/10.1038/nnano.2014.26

[64] A. Pospischil, M.M. Furchi and T. Mueller, Nat Nanotechnol. 9, 257 (2014). http://doi.org/10.1038/nnano.2014.14

[65] A. Polman, M. Knight, E.C. Garnett, B. Ehrler, and W.C. Sinke, Science. 352, aad4424 (2016). http://doi.org/10.1126/science.aad4424

[66] X. Wen, W. Wu and Z.L. Wang, Nano Energy. 2, 1093 (2013). http://doi.org/10.1016/j.nanoen.2013.08.008

[67] L. Zhu, P. Lin, B. Chen, L. Wang, L. Chen, D. Li, and Z.L. Wang, Nano Research. 11, 3877 (2018). http://doi.org/10.1007/s12274-017-1962-z

[68] J. Fujimura, Y. Adachi, T. Takahashi, and T. Kobayashi, Nano Energy. 99, (2022). http://doi.org/10.1016/j.nanoen.2022.107385

[69] G. Hu, W. Guo, R. Yu, X. Yang, R. Zhou, C. Pan, and Z.L. Wang, Nano Energy. 23, 27 (2016). http://doi.org/10.1016/j.nanoen.2016.02.057

[70] L. Zhu, L. Wang, F. Xue, L. Chen, J. Fu, X. Feng, T. Li, and Z.L. Wang, Adv Sci. 4, 1600185 (2017). http://doi.org/10.1002/advs.201600185

[71] C. Jiang, L. Jing, X. Huang, M. Liu, C. Du, T. Liu, X. Pu, W. Hu, and Z.L. Wang, ACS Nano. 11, 9405 (2017). http://doi.org/10.1021/acsnano.7b04935

[72] C. Jiang, Y. Chen, J. Sun, L. Jing, M. Liu, T. Liu, Y. Pan, X. Pu, B. Ma, W. Hu, and Z.L. Wang, Nano Energy. 57, 300 (2019). http://doi.org/10.1016/j.nanoen.2018.12.036

[73] H.S. Yun, B.w. Park, Y.C. Choi, J. Im, T.J. Shin, and S.I. Seok, Advanced Energy Materials. 9, (2019). http://doi.org/10.1002/aenm.201901343

[74] K.F. Abd El-Rahman, A.A.A. Darwish and E.A.A. El-Shazly, Materials Science in Semiconductor Processing. 25, 123 (2014). http://doi.org/10.1016/j.mssp.2013.10.003

[75] M. Feng, S.C. Liu, L. Hu, J. Wu, X. Liu, D.J. Xue, J.S. Hu, and L.J. Wan, J Am Chem Soc. (2021). http://doi.org/10.1021/jacs.1c04734

[76] S.C. Liu, C.M. Dai, Y. Min, Y. Hou, A.H. Proppe, Y. Zhou, C. Chen, S. Chen, J. Tang, D.J. Xue, E.H. Sargent, and J.S. Hu, Nat Commun. 12, 670 (2021). http://doi.org/10.1038/s41467-021-20955-5

[77] M. Shanmugam, R. Jacobs-Gedrim, E.S. Song, and B. Yu, Nanoscale. 6, 12682 (2014). http://doi.org/10.1039/c4nr03334e

[78] K. Nassiri Nazif, A. Daus, J. Hong, N. Lee, S. Vaziri, A. Kumar, F. Nitta, M.E. Chen, S. Kananian, R. Islam, K.H. Kim, J.H. Park, A.S.Y. Poon, M.L. Brongersma, E. Pop, and K.C. Saraswat, Nat Commun. 12, 7034 (2021). http://doi.org/10.1038/s41467-021-27195-7

[79] S. Wi, H. Kim, M. Chen, H. Nam, L.J. Guo, E. Meyhofer, and X. Liang, ACS nano. 8, 5270 (2014).

[80] J.P.B. Silva, C. Almeida Marques, A.S. Viana, L.F. Santos, K. Gwozdz, E. Popko, J.P. Connolly, K. Veltruska, V. Matolin, and O. Conde, Sci Rep. 10, 1215 (2020). http://doi.org/10.1038/s41598-020-58164-7

[81] Z. Li, B. Li, X. Wu, S.A. Sheppard, S. Zhang, D. Gao, N.J. Long, and Z. Zhu, Science. 376, 416 (2022).

[82] A. De Vos, Journal of Physics D: Applied Physics. 13, 839 (1980).

[83] F. Guo, N. Li, F.W. Fecher, N. Gasparini, C.O. Ramirez Quiroz, C. Bronnbauer, Y. Hou, V.V. Radmilovic, V.R. Radmilovic, E. Spiecker, K. Forberich, and C.J. Brabec, Nat Commun. 6, 7730 (2015). http://doi.org/10.1038/ncomms8730

[84] D.Q. Khoa, C.V. Nguyen, H.V. Phuc, V.V. Ilyasov, T.V. Vu, N.Q. Cuong, B.D. Hoi, D.V. Lu, E. Feddi, and M. El-Yadri, Physica B: Condensed Matter. 545, 255 (2018).

[85] Z. Nabi, A. Kellou, S. Mecabih, A. Khalfi, and N. Benosman, Materials Science and Engineering: B. 98, 104 (2003).

[86] R. Fei, W. Li, J. Li, and L. Yang, Applied Physics Letters. 107, 173104 (2015).

[87] L.C. Gomes, A. Carvalho and A.C. Neto, Physical Review B. 92, 214103 (2015).

[88] T.V. Vu, H.D. Tong, T.K. Nguyen, C.V. Nguyen, A. Lavrentyev, O. Khyzhun, B. Gabrelian, H.L. Luong, K.D. Pham, and P.T. Dang, Chemical Physics. 521, 5 (2019).

[89] S. Zhang, N. Wang, S. Liu, S. Huang, W. Zhou, B. Cai, M. Xie, Q. Yang, X. Chen, and H. Zeng, Nanotechnology. 27, 274001 (2016).

[90] A.Y. Shah, G. Kedarnath, A. Tyagi, C. Betty, V.K. Jain, and B. Vishwanadh, ChemistrySelect. 2, 4598 (2017).

[91] Y. Xu, H. Zhang, H. Shao, G. Ni, J. Li, H. Lu, R. Zhang, B. Peng, Y. Zhu, and H. Zhu, Physical Review B. 96, 245421 (2017).

[92] R. Chaurasiya, A. Dixit and R. Pandey, Superlattices and Microstructures. 122, 268 (2018). http://doi.org/10.1016/j.spmi.2018.07.039

[93] A. Hichri, I.B. Amara, S. Ayari, and S. Jaziri, Journal of Physics: Condensed Matter. 29, 435305 (2017).

[94] Y. Li, A. Chernikov, X. Zhang, A. Rigosi, H.M. Hill, A.M. Van Der Zande, D.A. Chenet, E.-M. Shih, J. Hone, and T.F. Heinz, Physical Review B. 90, 205422 (2014).

[95] K.-A.N. Duerloo, M.T. Ong and E.J. Reed, The Journal of Physical Chemistry Letters. 3, 2871 (2012). http://doi.org/10.1021/jz3012436

[96] H.J. Conley, B. Wang, J.I. Ziegler, R.F. Haglund Jr, S.T. Pantelides, and K.I. Bolotin, Nano letters. 13, 3626 (2013).

[97] Y. Zhou, W. Liu, X. Huang, A. Zhang, Y. Zhang, and Z.L. Wang, Nano Research. 9, 800 (2016).

[98] J.O. Island, A. Kuc, E.H. Diependaal, R. Bratschitsch, H.S. Van Der Zant, T. Heine, and A. Castellanos-Gomez, Nanoscale. 8, 2589 (2016).

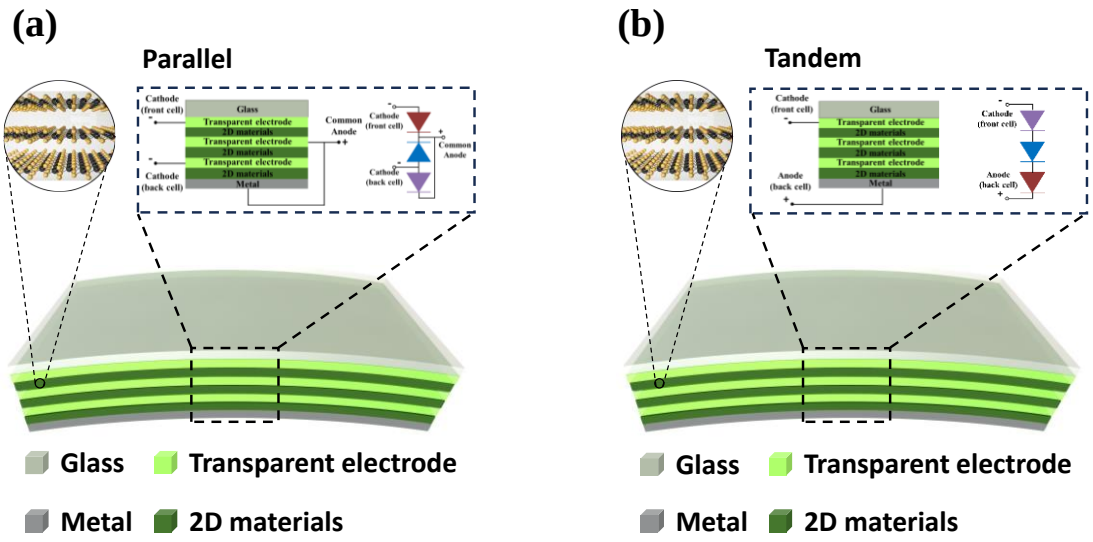
(a)
Parallel
Cathode (front cell)
Glass
Transparent electrode
2D materials
Transparent electrode
2D materials
Transparent electrode
2D materials
Metal
Cathode (back cell)
Common Anode
Cathode (front cell)
Common Anode
Cathode (back cell)
(b)
Tandem
Cathode (front cell)
Glass
Transparent electrode
2D materials
Transparent electrode
2D materials
Transparent electrode
2D materials
Metal
Anode (back cell)
Cathode (front cell)
Anode (back cell)
Glass
Transparent electrode
Metal
2D materials

Figure 1

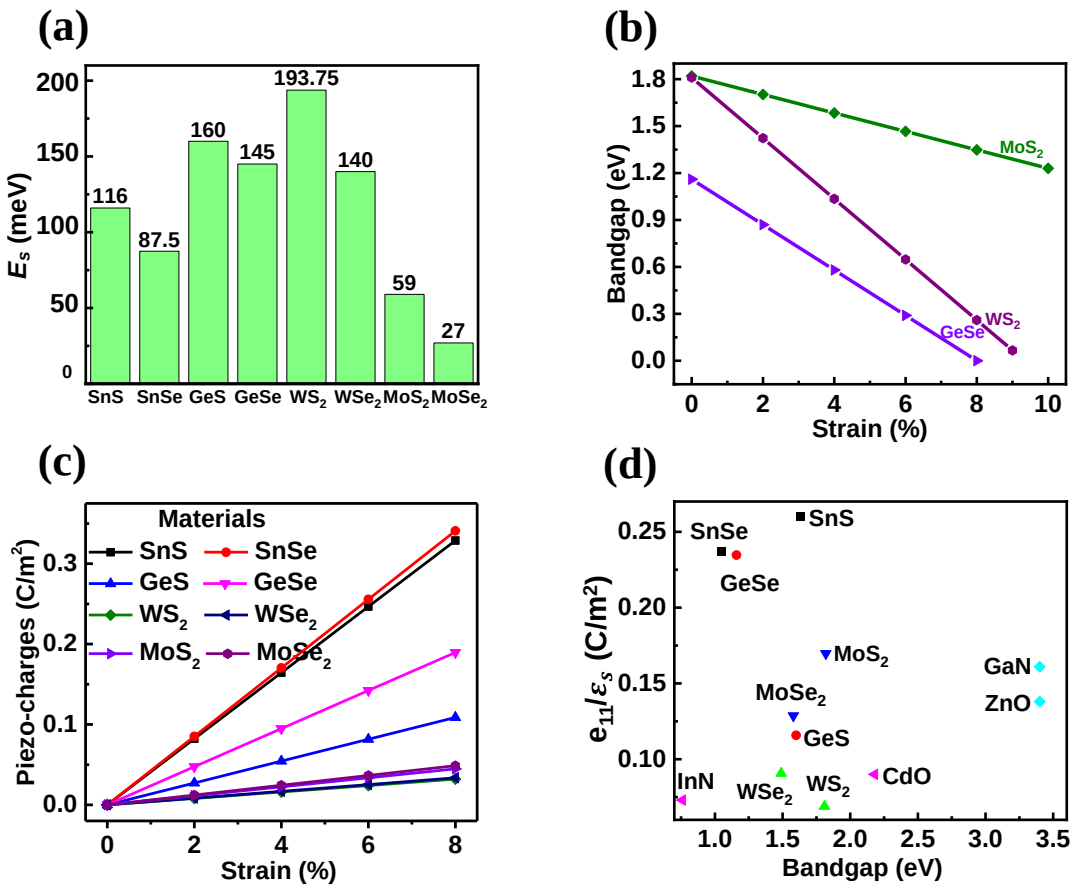
(a)
E_s (meV)
200
150
100
50
0
116
87.5
160
145
193.75
140
59
27
SnS
SnSe
GeS
GeSe
WS2
WSe2
MoS2
MoSe2
(b)
Bandgap (eV)
1.8
1.5
1.2
0.9
0.6
0.3
0.0
MoS2
WS2
GeSe
0
2
4
6
8
10
Strain (%)
(c)
Piezo-charges (C/m2)
0.3
0.2
0.1
0.0
Materials
SnS
SnSe
GeS
GeSe
WS2
WSe2
MoS2
MoSe2
0
2
4
6
8
Strain (%)
(d)
e11/εs (C/m2)
0.25
0.20
0.15
0.10
SnS
SnSe
GeSe
MoS2
GaN
ZnO
MoSe2
GeS
InN
WSe2
WS2
CdO
1.0
1.5
2.0
2.5
3.0
3.5
Bandgap (eV)

Figure 2

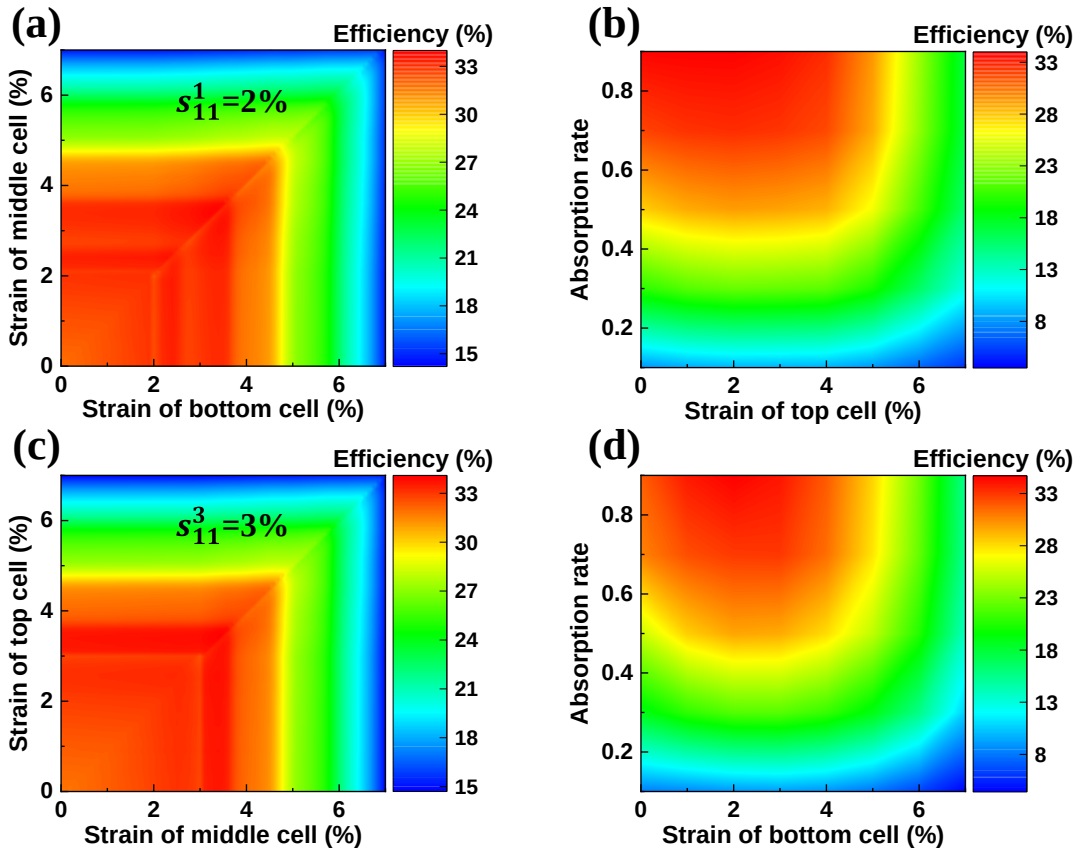
(a)
Efficiency (%)
s_{11}^{1}=2%
Strain of middle cell (%)
Strain of bottom cell (%)
(b)
Efficiency (%)
Absorption rate
Strain of top cell (%)
(c)
Efficiency (%)
s_{11}^{3}=3%
Strain of top cell (%)
Strain of middle cell (%)
(d)
Efficiency (%)
Absorption rate
Strain of bottom cell (%)

Figure 3

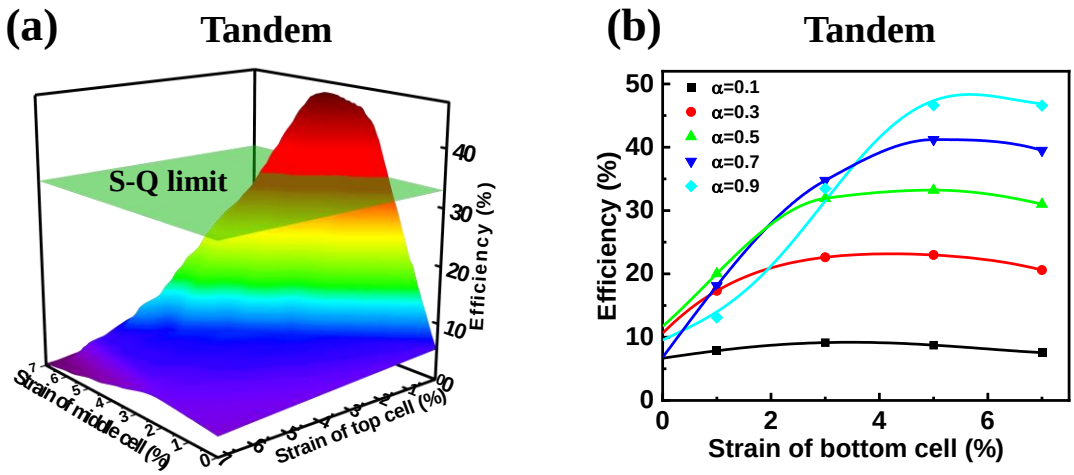
(a)
Tandem
S-Q limit
Efficiency (%)
Strain of middle cell (%)
Strain of top cell (%)
(b)
Tandem
α=0.1
α=0.3
α=0.5
α=0.7
α=0.9
Efficiency (%)
Strain of bottom cell (%)

Figure 4

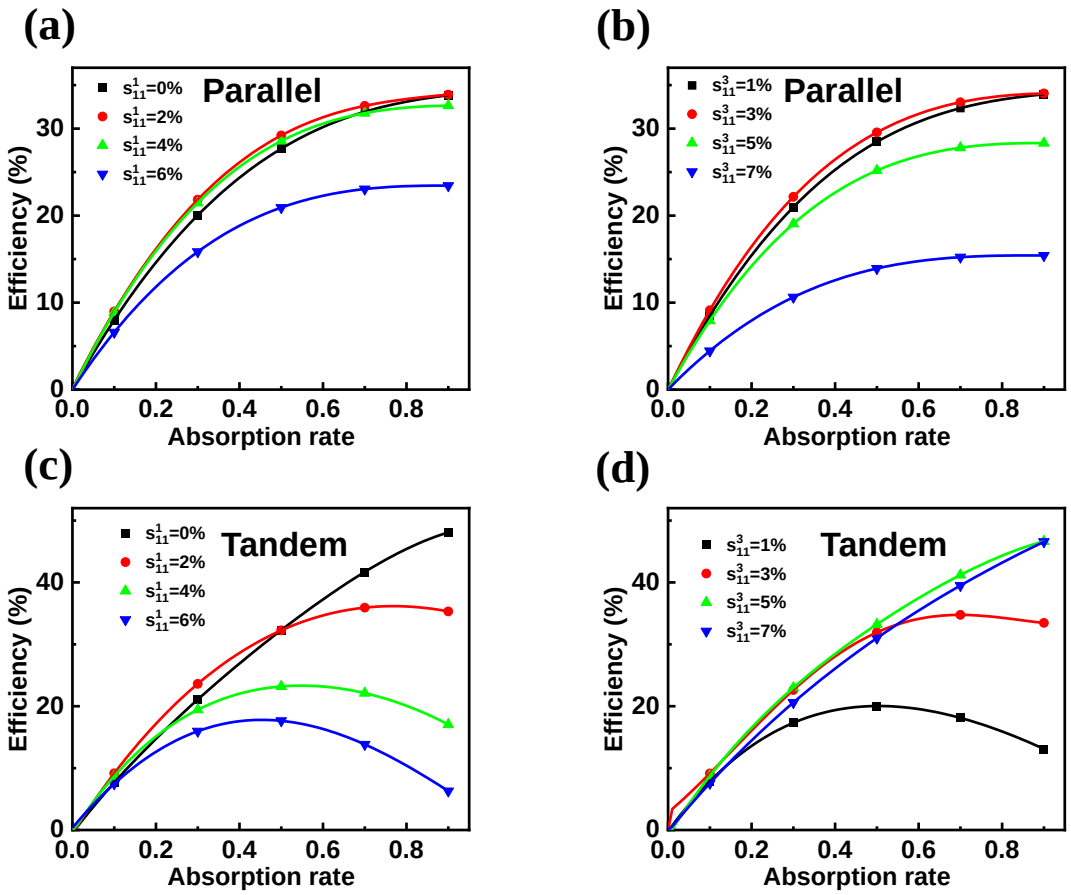
(a)
Parallel
s_{11}^1=0%
s_{11}^1=2%
s_{11}^1=4%
s_{11}^1=6%
Efficiency (%)
Absorption rate
(b)
Parallel
s_{11}^3=1%
s_{11}^3=3%
s_{11}^3=5%
s_{11}^3=7%
Efficiency (%)
Absorption rate
(c)
Tandem
s_{11}^1=0%
s_{11}^1=2%
s_{11}^1=4%
s_{11}^1=6%
Efficiency (%)
Absorption rate
(d)
Tandem
s_{11}^3=1%
s_{11}^3=3%
s_{11}^3=5%
s_{11}^3=7%
Efficiency (%)
Absorption rate

Figure 5

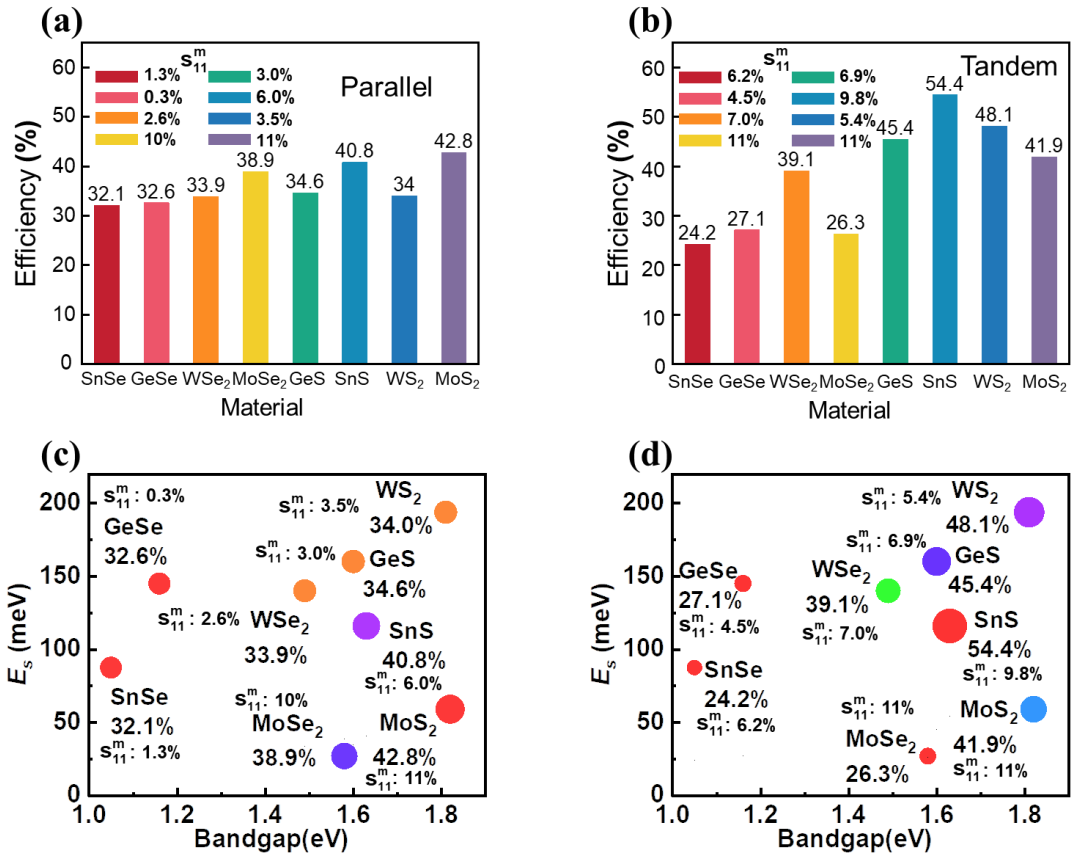
(a)
Parallel
Efficiency (%)
Material
SnSe GeSe WSe2 MoSe2 GeS SnS WS2 MoS2
32.1 32.6 33.9 38.9 34.6 40.8 34 42.8
(b)
Tandem
Efficiency (%)
Material
24.2 27.1 39.1 26.3 45.4 54.4 48.1 41.9
(c)
Es (meV)
Bandgap(eV)
(d)
Es (meV)
Bandgap(eV)

Figure 6